Catal Lett (2012) 142:753–762
DOI 10.1007/s10562-012-0800-x

Investigation of the Stability of CeO_2, V_2O_5 and CeV Mixed Oxide on the Partial Oxidation of Propane

Carlos Alberto Chagas · Lidia Chaloub Dieguez · Martin Schmal

Received: 19 January 2012 / Accepted: 1 March 2012 / Published online: 5 April 2012

Abstract The cerium–vanadium mixed oxide was synthesized by complexation method. XRD patterns of the (CeV) mixed oxide showed the formation of $CeVO_4$ phase and segregated CeO_2. Incorporation of vanadium into the ceria structure improved the redox ability of ceria. The results showed that the activity of the (CeV) mixed oxide was higher than of the vanadium oxide (V_2O_5) for the partial oxidation of propane. Both catalysts showed similar hydrogen selectivity but significant deactivation with time on stream. Investigation by XRD diffractograms of V_2O_5 after reaction showed sintering of V_2O_5 and different oxidation states after reaction, while the crystallites and the structure of the mixed oxide $CeVO_4$ remained unchanged. The deactivation of the mixed oxide (CeV) with time on stream can be explained by insufficient oxygen supply to restore the CeO_2 species at the surface.

Keywords Hydrogen · Propane · Partial oxidation · Vanadium oxide · Cerium oxide · CeV mixed oxide

1 Introduction

Hydrogen is important in oil refineries and in chemical industries, and it is becoming attractive for fuel cells and combustion engines [1, 2]. Moreover, hydrogen offers a potentially non-polluting, inexhaustible, efficient, and cost attractive fuel for energy demands. The use of hydrogen as a fuel offers an important reduction in NO_x, CO, and CO_2 emissions, when non-fossil fuels are used for the production of hydrogen [2]. Typically, hydrogen production is carried out by steam reforming, autothermal reforming, or partial oxidation of methane or ethanol [3]. The partial oxidation of light hydrocarbons, among others propane or mixtures of propane and butane (LPG), is particularly advantageous when system compactness is the main target. Upon considering the several primary fuels, propane is an attractive option since it is a primary constituent of liquefied petroleum gas (LPG) that is increasingly used as a substitute for gasoline and diesel in transport vehicles [4].

Although relatively scarce, the literature presents different types of catalysts for hydrogen generation for the partial oxidation of propane. Commonly these supported catalysts contain noble metals as active phases, such as: Rh [5], Pt [6, 7] and Pd [8] or even non-noble metals such as Ni [6, 9, 10], although the last one is more sensitive to carbon formation [11]. The catalysts based on noble metals present good activity and excellent resistance to carbon formation, but high costs for commercial usage. In this context, there is a good possibility of using mixed oxides as alternative for H_2 generation. In addition, mixed oxides have high mobility of oxygen, or redox property [12], high oxygen storage capacity [13], besides lower costs compared to the noble metals and less susceptible carbon formation than Ni based catalysts. Recent papers confirm that considerable amounts of H_2 are produced with vanadium and cerium oxide based catalysts, under conditions that are typically employed for partial oxidation of propane [14, 15].

The objective of the present work is to investigate the stability of the V_2O_5, CeO_2 and of the mixed oxide (CeV) for the partial oxidation of propane under sub-stoichiometric feed O_2/C_3H_8 condition. The selectivity and stability of the CeV was also studied and compared with the

C. A. Chagas · L. C. Dieguez · M. Schmal (✉)
Programa de Engenharia Química-COPPE/NUCAT,
Centro de Tecnologia, Federal University of Rio de Janeiro,
Bl. G 128, P.O. Box 68502, Rio de Janeiro, RJ 21941-972, Brazil
e-mail: schmal@peq.coppe.ufrj.br

performance of isolated oxides V_2O_5 and CeO_2. XRD analysis of fresh and used catalysts was used for evaluation of phase and structural changes during the reaction.

2 Experimental

2.1 Catalyst Preparation

$Ce_xV_yO_z$ mixed oxide (CeV) was prepared by complexation method according to Yasyerli et al. [16]. In this method, cerium nitrate hexahydrate ($Ce(NO_3)_3$ $6H_2O$, 0.98 mol) and ammonium monovanadate (NH_4VO_3, 0.14 mol) were used as precursors, and citric acid (2.1 mol) as complexation agent. The CeV mixed oxide was prepared for an atomic ratio Ce/V = 1. Pure CeO_2 was prepared by precipitation of cerium nitrate hexahydrate ($Ce(NO_3)_3$ $6H_2O$, 0.2 mol). The precipitate was filtered, washed with deionized water, dried overnight at 110 °C and then calcined in air flow at 500 °C for 5 h. The V_2O_5 catalyst was commercial sample (Aldrich) used as reference.

2.2 Catalyst Characterization

The specific surface area and textural properties of the catalysts were measured by nitrogen adsorption–desorption at −196 °C, using the ASAP apparatus, model 2020 (Micromeritics). The samples were priori degassed at 300 °C for 24 h.

The elemental chemical composition of the mixed oxide (CeV) was determined by X-ray fluorescence spectroscopy (XRF) using a Rigaku RIX 3100 apparatus. X-ray diffraction (XRD) of powder samples were performed on a Rigaku model Miniflex apparatus, using CuK_α $\lambda = 1.5418$ Å. Data were collected for 2θ between 10 and 80° with a step size of 0.05° and a counting time of 1.0 s $step^{-1}$. The XRD data of mixed oxide (CeV) were treated by the Rietveld method [17], quantifying the crystalline phases by using the software FULLPROF 98®.

SEM images were recorded in a field emission gun scanning electron microscope (FEG–SEM–FEI Company, model QUANTA 400). The thermogravimetric analysis was performed on a thermal analyzer (Rigaku TAS-100) under nitrogen flow at a heating rate of 10 °C min^{-1}.

The redox properties and redox reversibility of the synthesized CeV and CeO_2 were determined by temperature programmed reduction (TPR) and temperature programmed oxidation (TPO) successively. The TPR and TPO experiments were conducted with 1.53 vol.% H_2/Ar and 5 vol.% O_2/He flow at 30 mL min^{-1}, respectively, with increasing temperature from room temperature up to 900 °C. These experiments were performed using a quartz U-tube reactor, coupled to a thermal conductivity detector (TCD). Prior reduction the samples (0.1 g) were dried at 150 °C during 0.5 h, under argon flow (AGA, 99.99 %).

The temperature-programmed surface reaction (TPSR) analysis was performed in micro glass tube reactor at atmospheric pressure. The catalyst (0.3 g) was pretreated with pure helium at 200 °C during 1 h. Then, a reaction mixture containing 20 vol.% O_2, 20 vol.% C_3H_8 balanced with He flew through the catalyst, raising the temperature at 10 °C min^{-1} from room temperature up to 500 °C. The exit gases were monitored continuously by a quadrupole mass spectrometer (Balzers Prisma-QMS 200).

2.3 Partial Oxidation of Propane

Catalytic tests for the partial oxidation of propane were carried out in a fixed-bed quartz tube reactor under atmospheric pressure and at 500 °C. The mass of catalyst was 0.2 g and the feed composition was $C_3H_8/O_2/He$ = 10/10/80 ($O_2/C_3H_8 = 1$). The contact time (W/F) was 1.7×10^{-3} g_{cat} min cm^{-3}. Before testing, the catalyst was pretreated with a helium flow at 200 °C for 1 h. The CeO_2 sample was pretreated with a 20 vol.% O_2/He flow at 400 °C for 1 h. Preliminary tests were carried out to ensure kinetic reaction conditions. The thermal stability was also tested before reaction. The effluent gases were analyzed by gas chromatography (CP-3800) and TCD. Two columns were used, PoraPlot-Q and Sieve Molecular 5A. Finally, after reaction the catalysts were analyzed by XRD.

3 Results

3.1 Textural Properties

The N_2 adsorption–desorption isotherms for all catalysts, are of type II, typical for macroporous solids, with a final upwards tail suggesting the presence of mesopores. All catalysts showed H3 type hysteresis, indicating formation of aggregates or agglomerated particles as slit shaped pores (plates or edged particles like cubes) [18].

The textural properties of the catalysts obtained from the adsorption–desorption isotherms are listed in Table 1. All catalysts showed pore sizes between 20 and 500 Å, characteristic of mesoporous materials [18]. However, the

Table 1 Physical properties of the catalysts

Catalysts	BET surface area (m^2 g^{-1})	Pore volume (cm^3 g^{-1})	Average pore size (Å)
V_2O_5	<10	0.013	151
CeO_2	45	0.101	89
CeV	15	0.104	283

isotherms showed the existence of macro and mesopores. The BET surface areas of vanadium and cerium oxides agreed with the reported values in the literature [16, 19].

The elemental analysis from XRF data revealed the presence of pure mixed oxide ($CeVO_4$) with an atomic ration Ce/V = 1.1. According to the literature [16] if the atomic ratio Ce/V is higher than 1 then the cerium oxide is in excess, leading to formation of segregated phases of CeO_2.

3.2 XRD

Figure 1 shows the XRD patterns of all catalysts. The vanadium oxide showed the most intense diffraction line at $2\theta = 26.13°$, compared to the database JCPDS41-1426 (I = 75 % at $2\theta = 26.13°$ related to the (110) reflection plane). This occurred probably during analysis, due to a possible orientation of the sample, where the structure of the vanadium oxide is of type layer. The synthesized cerium oxide showed a diffraction pattern of pure CeO_2 phase (JCPDS34-394) with diffraction lines of high intensity (I = 100 %) at $2\theta = 28.85°$, corresponding the (111) reflection and fluorite structure with space group *Fm3m*.

The mixed oxide indicates the $CeVO_4$ phase according to JCPDS12-757, with diffraction lines with high intensity at $2\theta = 24.26°$, corresponding the (200) reflection and tetragonal structure with space group I41/amd. However, analyzing the diffraction pattern of the mixed oxide, we also observe characteristic diffraction lines of CeO_2 (JCPDS34-394), indicating the formation of segregated CeO_2 phase.

The XRD data of the mixed oxide (CeV) was analyzed by Rietveld method, as shown in Fig. 2. There is a good correlation between experimental data and simulated curve, as indicated by the difference between the profiles (curve $Y_{obs}–Y_{cal}$). The results revealed the presence of 87 % of $CeVO_4$ phase and 13 % of CeO_2 phase, which are in good agreement with the X-ray fluorescence spectroscopy results. Table 2 shows the average crystallite sizes, calculated from the diffraction line broadening, using the Scherrer's equation, after Rietveld refinement. Table 2 show that the mixed oxide and the vanadium oxide have similar crystallite sizes, whereas the cerium oxide much lower sizes.

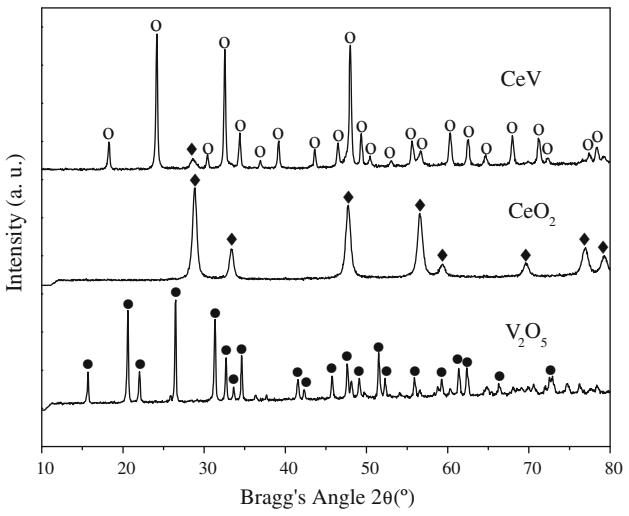

Fig. 1 XRD patterns of the CeV and CeO_2 catalysts. Symbols: (*zero*) $CeVO_4$ (JCPDS12-757), (*diamond*) CeO_2 (JCPDS34-394) and (*bullet*) V_2O_5 (JCPDS41-1426)

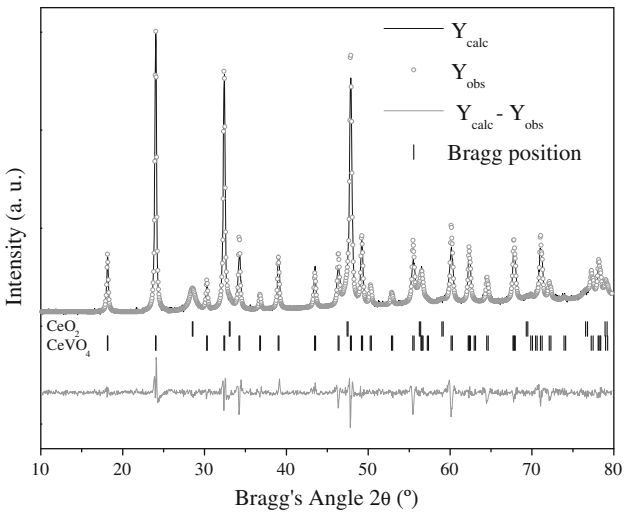

Fig. 2 Rietveld refinement of CeV catalysts. Experimental data are indicated by *circles* and the *continuous line* is the calculated curve after refinement. The *lower curve* represents the difference between the experimental data and the calculated curve

Figure 3 displays SEM micrographs images of the mixed oxide (CeV) and of the cerium and vanadium oxides samples. These pictures show significant textural and morphological differences of the mixed oxide and the isolated CeO_2 and V_2O_5 oxides.

The EDS semi-quantitative analyses and chemical mapping of the mixed oxide images are shown in Fig. 4. They revealed excellent distribution of the metals, suggesting a homogeneous chemical composition. The atomic ratio of Ce/V, obtained from EDS analysis, was 1.1, in good agreement with the X-ray fluorescence spectroscopy and refinement results.

Table 2 Crystallite parameters of the mixed oxides (CeV) after Rietveld calculations

Catalysts	(hkl)[a]	d_{hkl} (nm)[b]	L (nm)[c]
V_2O_5	(001)	0.429	37.2 ± 3.4
CeO_2	(111)	0.309	14.0 ± 5.0
CeV	(200)	0.366	32.2 ± 1.1

[a] Miller indices, [b] interplanar distance, [c] crystallite size

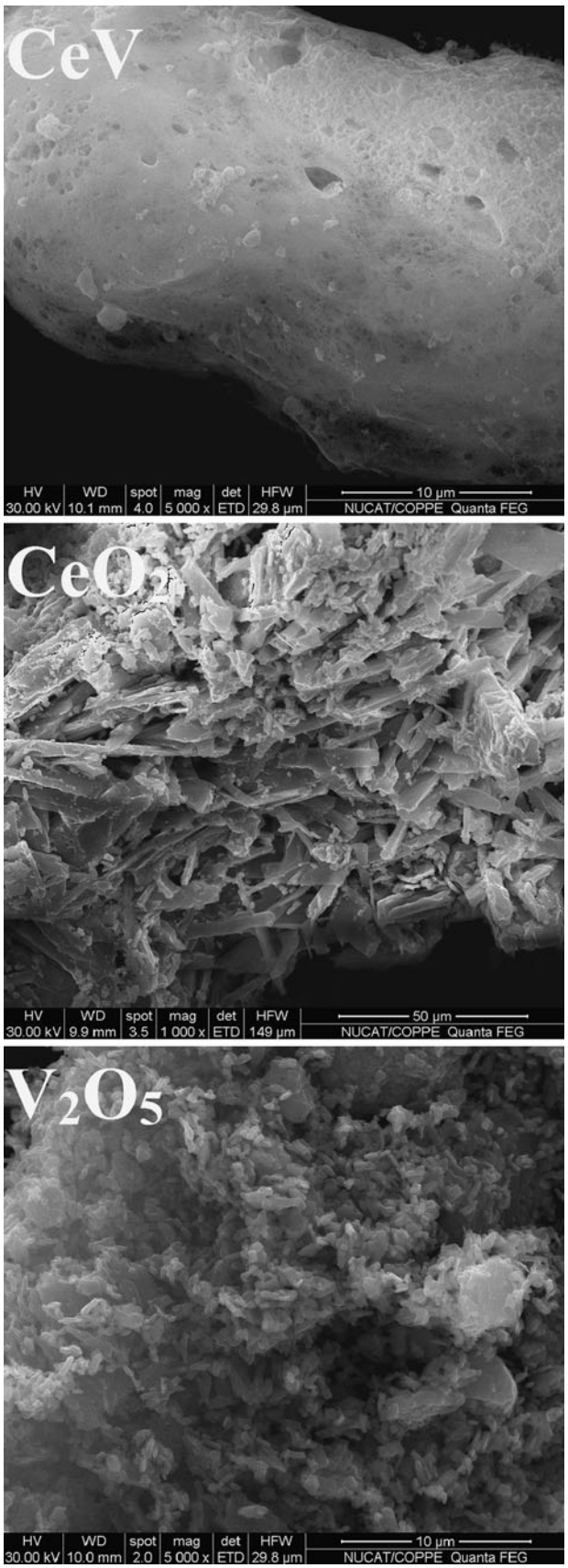

Fig. 3 SEM micrographs of all catalysts

3.3 Redox Property and Redox Reversibility of the CeO_2 and the Mixed Oxide (CeV)

The redox property of the CeO_2 and the mixed oxide (CeV) was investigated by the temperature-programmed reduction (TPR-1) and temperature-programmed oxidation (TPO) and again new reduction (TPR-2) after oxidation. The sample was reduced with a 1.53 vol.% H_2/Ar mixture flow, rising the temperature at 10 °C min^{-1} up to 900 °C. After passing a He flow for 30 min at this temperature and cooling to room temperature the feed gas was switched to a 5 vol.% O_2/He flow and temperature raised at 10 °C min^{-1} from room temperature up to 900 °C (TPO). Finally, a second TPR-2 was performed under reducing condition. Figure 5 displays the profiles of the hydrogen consumption for both catalysts. The TPR profiles (TPR-1 and TPR-2) of the mixed oxide were similar, but not for the CeO_2 between 400 and 600 °C.

Table 3 presents the amounts of O_2 chemissorbed and H_2 uptake (from TPR-1 and TPR-2). The hydrogen consumption of the second reduction (TPR-2) for both catalysts was approximately equal to the first reduction (TPR-1) after oxidation, which indicates redox reversibility. These results are consistent with CeO_2 values reported by Laosiripojana et al. [15, 20]. Notwithstanding is the higher hydrogen consumption of the mixed oxide (CeV) compared to the CeO_2, as shown in Table 3, suggesting higher oxygen storage capacities (OSC).

3.4 Temperature Programmed Reaction Analysis (TPSR)

The TPSR profiles with increasing temperature from 25 to 500 °C of the V_2O_5 sample are displayed in Fig. 6a. Under these reaction conditions, oxygen was the limiting reactant. The reaction started at 450 °C and showed a maximum CO and minimum C_3H_8 formation at 470 °C, displaying two significant domains. Between 450 and 470 °C, the O_2 concentration decreased until almost complete consumption, with increasing CO and CO_2 formation, which implies simultaneously occurrence of total propane oxidation (Eq. 1) and WGSR (Eq. 2) due to the formation of H_2 in this region.

$$C_3H_8 + 5O_2 \rightarrow 3CO_2 + 4H_2O \quad \Delta H_{298} = -2046 \text{ kJ mol}^{-1} \tag{1}$$

$$CO + H_2O \rightarrow CO_2 + H_2 \quad \Delta H_{298} = -41.09 \text{ kJ mol}^{-1} \tag{2}$$

In the second region, above 470 °C, H_2 formation increased together with a significant consumption of CO and CO_2, notwithstanding the total oxygen conversion. The propane conversion decreased above 470 °C, although H_2 formation. The H_2 formation is attributed to the partial

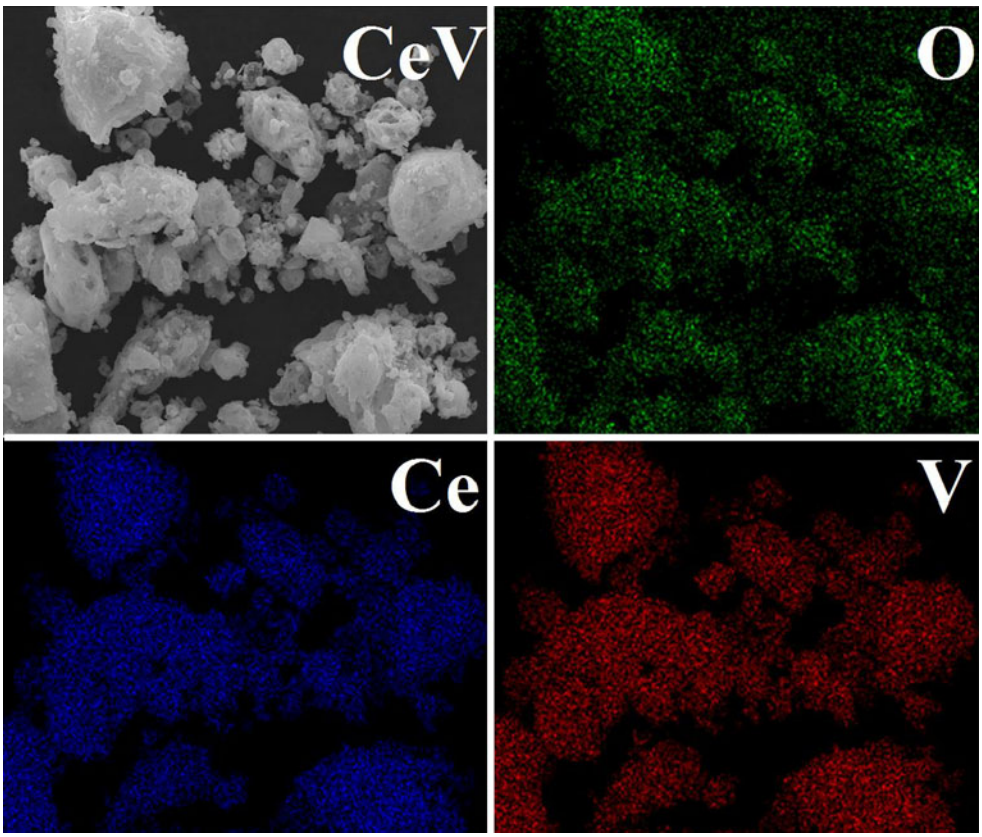

Fig. 4 EDS/SEM analysis of CeV catalyst

oxidation of propane (Eq. 3) but preferentially by steam reforming (Eqs. 4, 5) due to the water formation in the first step, besides the Boudouard reaction (Eq. 6).

$$C_3H_8 + 1.5O_2 \rightarrow 3CO + 4H_2 \quad \Delta H_{298} = -229 \text{ kJ mol}^{-1} \tag{3}$$

$$C_3H_8 + 3H_2O \rightarrow 3CO_2 + 7H_2 \quad \Delta H_{298} = 497 \text{ kJ mol}^{-1} \tag{4}$$

$$C_3H_8 + 6H_2O \rightarrow 3CO_2 + 10H_2 \quad \Delta H_{298} = 395 \text{ kJ mol}^{-1} \tag{5}$$

$$2CO \rightarrow C_{(S)} + CO_2 \quad \Delta H_{298} = -172 \text{ kJ mol}^{-1} \tag{6}$$

The mixed oxide CeV presented a different behavior in the TPSR experiment, as shown in Fig. 6b. The reaction started also about 450 °C with the consumption of propane in less extend and higher consumption of oxygen, with simultaneous formation of CO_2, CO and H_2. It does not exhibit a maximum conversion, as seen in the previous case, and occurs only between 450 and 500 °C, suggesting a different reaction path, when compared to the V_2O_5 sample. Notwithstanding is that in this region the H_2 formation was not accompanied with the CO and CO_2 consumption, and on the contrary, they increased almost till 500 °C. For the identification of the reactions giving rise to hydrogen formation above 455 °C, a balance between the amount of each product must be considered and under such conditions, part of the hydrogen was produced by dehydrogenation of propane to propylene (in fact, the conversion of propane increased even after total oxygen conversion had been reached), and probably by coke formation (Eqs. 7, 8)

$$C_3H_8 \rightarrow C_3H_6 + H_2 \quad \Delta H_{298} = 124 \text{ kJ mol}^{-1} \tag{7}$$

$$C_3H_8 \rightarrow 3C + 4H_2 \quad \Delta H_{298} = 104 \text{ kJ mol}^{-1} \tag{8}$$

$$C_3H_8 + 3CO_2 \rightarrow 6CO + 4H_2 \quad \Delta H_{298} = 620 \text{ kJ mol}^{-1} \tag{9}$$

The dry reforming of propane (Eq. 9) explains the simultaneous formation of CO and H_2 with increasing temperature. Moreover, the formation of CO with increasing temperature can also be assigned to the reverse WGSR (Eq. 2), not occurring on the vanadium catalyst.

As reported previously [14, 19] the WGSR occurs on the reduced V_2O_3 species at high temperature, in the absence of the gas-phase oxygen. The vanadium sesquioxide was found to be the effective active species for the WGSR, while V_2O_5 was inactive.

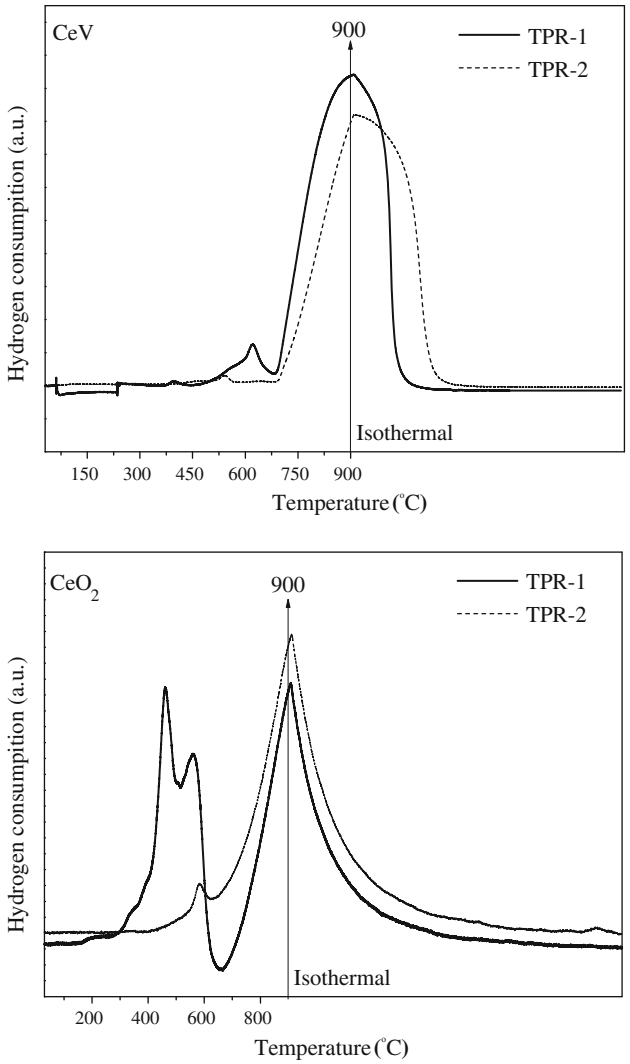

Fig. 5 Temperature-programmed reduction profiles (TPR-1 and TPR-2) of CeV and CeO_2, respectively

Table 3 TPR-1, TPO and TPR-2: H_2 and O_2 consumption of CeO_2 and CeV catalysts

Catalysts	Total H_2 uptake from TPR-1 (μmol g^{-1})	Total O_2 uptake from TPO (μmol g^{-1})	Total H_2 uptake from TPR-2 (μmol g^{-1})
CeO_2	1342	653	1212
CeV	3618	1798	3641

The results observed for the V_2O_5 catalysts are in good agreement with those obtained by Ballarini et al. [14]. However, they observed the maximum at 400 °C with similar reactions in different regions.

3.5 Catalytic Activity

The equilibrium composition for the partial oxidation of propane under sub-stoichiometric conditions was calculated. The simulated inlet gas was similar as the feed composition (10 vol.% C_3H_8, 10 vol.% O_2 and 80 vol.% He). Table 4 presents the molar composition and the selectivity for 500 °C and 1 atm and for $O_2/C_3H_8 = 1$. As shown in the Table 4, the propane conversion was ~93% (mol). The amount of hydrogen at equilibrium is 53 % mol (on dry basis). Thus, tests were performed far from equilibrium condition.

Figure 7 show propane and oxygen conversions with time on stream for $O_2/C_3H_8 = 1$ and at 500 °C for all catalysts. The initial propane conversion was similar for all catalysts around 23–24 %, however, decreased by 1/3 after 30 min for the V_2O_5 sample.

The behavior of oxygen conversion was very different for each sample. For the V_2O_5 sample the initial conversion was 85 %, but decreased quickly in the first 30 min. Then it was constant around 35 % following the same trend of the propane conversion for 3 h. Thus, it became stable for longer times. On the other hand, the oxygen conversion of CeO_2 was 100 % for all time (3 h), following also the same trend of propane conversion, suggesting very stable catalyst for the partial oxidation of propane.

The mixed oxide CeV presented completely different behavior. The propane conversion decreased after 60 min and reached the same low conversion of the V_2O_5 sample while the oxygen conversion, initially high (100 %) decreased abruptly till 140 min and then became constant for longer periods. This behavior is unlikely, unexpected and deserved further investigation. The V_2O_5 catalyst used for comparison presented similar activity as reported in the literature [14, 19].

Figure 8 presents the selectivity for hydrogen with time on stream for all catalysts at isoconversion at 500 °C. The selectivity of the mixed oxide CeV and V_2O_5 were much higher than of CeO_2. The initial selectivity on CeV was higher and stabilized around 26 % after 120 min, compared to the selectivity of the V_2O_5 that decreased drastically but stabilized at 16 %. The CeO_2 exhibited very low selectivity around 7 %. These results suggest different surface reaction occurring under similar reaction conditions.

4 Discussion

The hydrogen formation is relevant but depends on the oxygen conversion with increasing temperature. Therefore, according to Ballarini et al. [14] there are two possible interpretations. 1) hydrogen formation was consecutive to the formation of other product reactions or 2) the nature of the surface affected the active sites for the oxygen and reactants during the reaction, influencing the product distribution [14]. This is the case when we compare the results of pure oxides with the mixed oxide. According to Ballarini

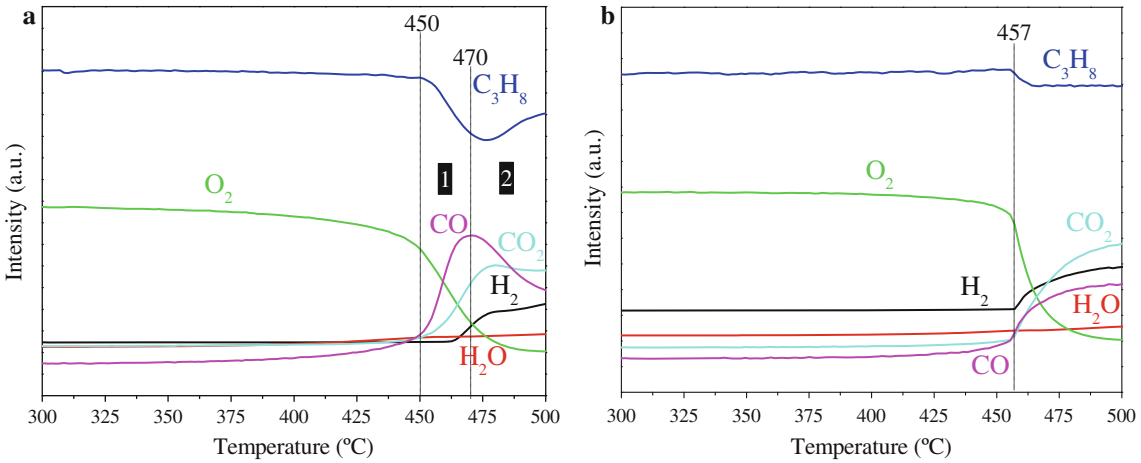

Fig. 6 TPRS profiles for the samples V_2O_5 (**a**) and CeV (**b**): feed conditions (10 vol.% CO/He, 10 vol.% O_2/He balanced with He)

Table 4 Thermodynamic composition simulation for the partial oxidation of propane

Compounds	Composition (% mol)	Selectivity (% mol)
C_3H_8	7.4	–
O_2	0	–
H_2	52.8	57
CO	38.6	41.7
CO_2	1.2	1.3

et al. [14] there is an important effect of the residence time. Above 1.5 s it is not significantly modified. In our TPSR experiments the residence time of the vanadium catalyst is of the order of 0.2 s, which corresponds to selectivity of the order of 20 %, and conversion of 30 %, in good agreement with Ballarini et al. [14].

The CeO_2 was the most active and stable with time on stream. This stability can be attributed to OSC, which favors the elimination of carbon deposition during propane dissociation. As well known the CeO_2 supplies mobile oxygen (O_O^x) from the vacancies to oxidize gaseous hydrocarbons [15].

The TPSR results showed that the dehydrogenation of propane to propylene and hydrogen occurs preferentially on the CeV and V_2O_5 catalysts and the total oxidation on cerium oxide. According to the literature [15], the partial oxidation of light hydrocarbons is attributed to the redox phenomena of these catalysts, as observed on the TPR results.

As seen the mixed oxide was apparently deactivated with time on stream, but became stable after some time. This deactivation could be attributed to the carbon deposition for such reaction conditions. Therefore, the CeV catalyst was submitted to a TGA after reaction tests. The results revealed that the mass loss was negligible.

During the reforming process, the gas–solid reactions between the hydrocarbons present in the system (i.e. propane, ethane, ethylene, and methane) and the lattice oxygen (O_O^x) take place on the mixed oxide, surface, reducing the degree of carbon deposition on the catalyst surface (from hydrocarbons decomposition and Boudouard reactions).

4.1 XRD After Catalytic Test

If carbon deposition occurs in less extend, the changes observed with time on stream on CeV and V_2O_5 catalysts must be explained by analyzing the structure modification after reaction. Therefore, the best technique for such analysis is the XRD. The analysis was performed after catalytic tests and results are displayed in Fig. 9(top). Indeed, for V_2O_5 catalyst after reaction at 500 °C, vanadium oxides in different oxidation states (namely V_2O_5, VO_2, V_2O_3, and possible traces of V_6O_{13}) were observed, confirming reported results of Ballarini et al. [14, 19]. Thus, the partial oxidation of propane for these reaction conditions transforms the vanadium oxide structure during the reaction, affecting electronic structures of the molecules and therefore, the adsorption properties on the surface and the reaction. Ballarini et al. [14, 19]. showed that the bulk vanadium oxide is not selective for the propane ODH, depending on the oxygen conversion and temperature. According to them V_2O_3 was more active than V_2O_5 and since V_2O_3 is hardly reducible the conversion is related to the ability in the activation of molecular oxygen and adsorption of intermediate species. It seems that the most important is the concentration of oxidizing sites. These authors claim that the more oxidized metal oxide favors the selectivity to products of combustion, and on the opposite for reduced oxides it favors the selectivity to products of partial oxidation. In our case, the oxygen conversion for the V_2O_5 sample was lower after 30 min compared to the

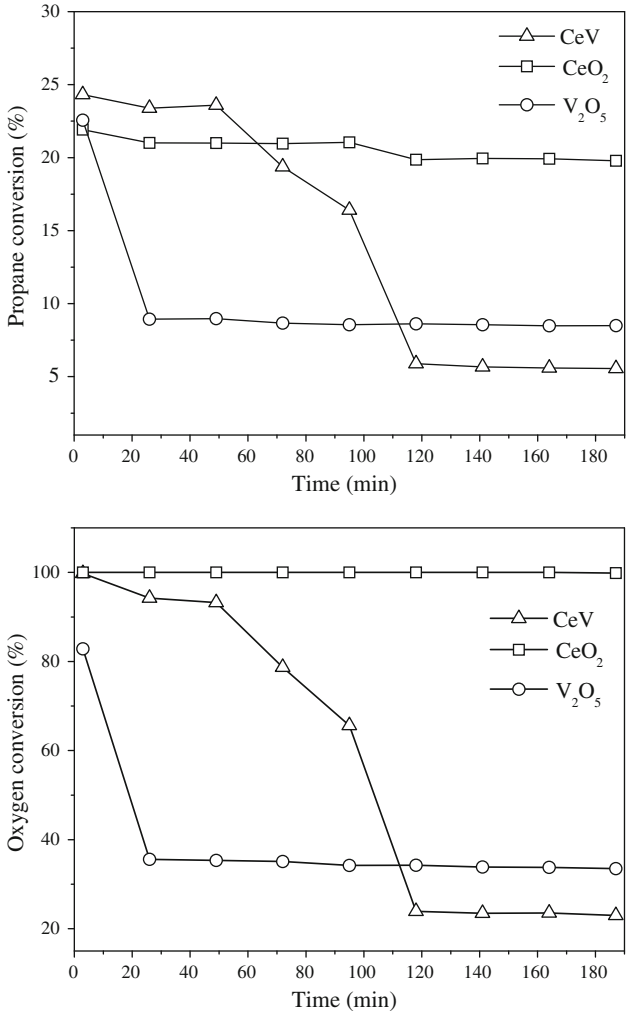

Fig. 7 Conversion of propane and oxygen with time on stream: (*triangle*) CeV, (*square*) CeO_2 and (*circle*) V_2O_5. Feed composition $C_3H_8/O_2/He = 10/10/80$ ($O_2/C_3H_8 = 1$): contact time (W/F) = 1.7×10^{-3} g_{cat} min cm^{-3} and T = 500 °C

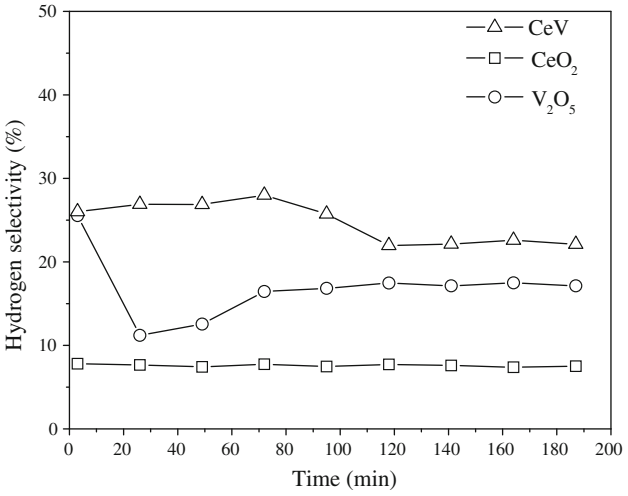

Fig. 8 Hydrogen selectivity with time on stream: (*triangle*) CeV, (*square*) CeO_2 and (*circle*) V_2O_5

initial conversion and therefore the surface active sites were modified, changing the reaction mechanism. Therefore, the reduction of V_2O_5 with time occurs on stream to V_2O_3 because abstraction the ionic oxygen decreased the propane conversion. The lower conversion of oxygen indicates the progressive reduction of V_2O_5 into V_2O_3 under these conditions and therefore the formation of surface species that favors the stability of the catalyst even at lower conversion levels.

Diffractograms of fresh and used mixed oxide (CeV) catalyst are presented in Fig. 9(bottom), showing similar diffraction patterns. However, with Rietveld refinement procedures the mean crystallite sizes were calculated by Scherrer equation, using the full width at half maximum of the peak at 24.26°, which corresponds to (200) plane of the CeV. Table 5 presents the results after reaction at 500 °C. Comparing the results before and after reaction (Tables 2 and 5) the crystallite sizes of V_2O_5 increased (37.2–54.4 nm) but of the mixed oxide CeV remained unchanged (32.2–39.8 nm). Therefore, crystallite sizes of V_2O_5 influenced significantly the abruptly decreasing initial activity and selectivity, which explains the sharp deactivation in Fig. 9 and confirms the structural modification, in accordance with Ballarini et al. [14, 19].

However, the unchanged crystallites sizes before and after reaction of the CeV does not explain the deactivation occurring with time on stream, but suggest modification of the surface reaction mechanism.

The oxygen storage capability of the mixed oxide (CeV) enhanced by a factor of 3, compared to the bulk CeO_2, as seen in Table 3. This result is equal to the reported value for the undoped mixed Ce-ZrO_2, which confirms the proposition presented by Laosiripojana et al. [20], even at very high reaction temperature (850 °C), close to the equilibrium condition. They claim that during the partial oxidation the gas–solid reaction between the hydrocarbon and the lattice oxygen O^{2-} takes place at the surface of the mixed oxide. The presence of the hydrocarbon implies the continuous removal of ionic oxygen that produces oxygen compounds like CO, CO_2 and H_2O and reduces the CeO_2 into Ce_2O_3.

However, contrary to Laosiripojana et al. [20] we observed here for lower reaction temperature (500 °C) and far from the equilibrium condition that with increasing time on stream, the catalytic performance was unstable. As shown in Figure 7 the conversion of oxygen decreases significantly with time on stream.

We performed Raman spectroscopy on fresh and after reaction mixed oxide (CeV) samples. From the spectra (not shown) of the fresh sample we observed a peak around 500 cm^{-1}, corresponding to the band 463 cm^{-1} of CeO_2

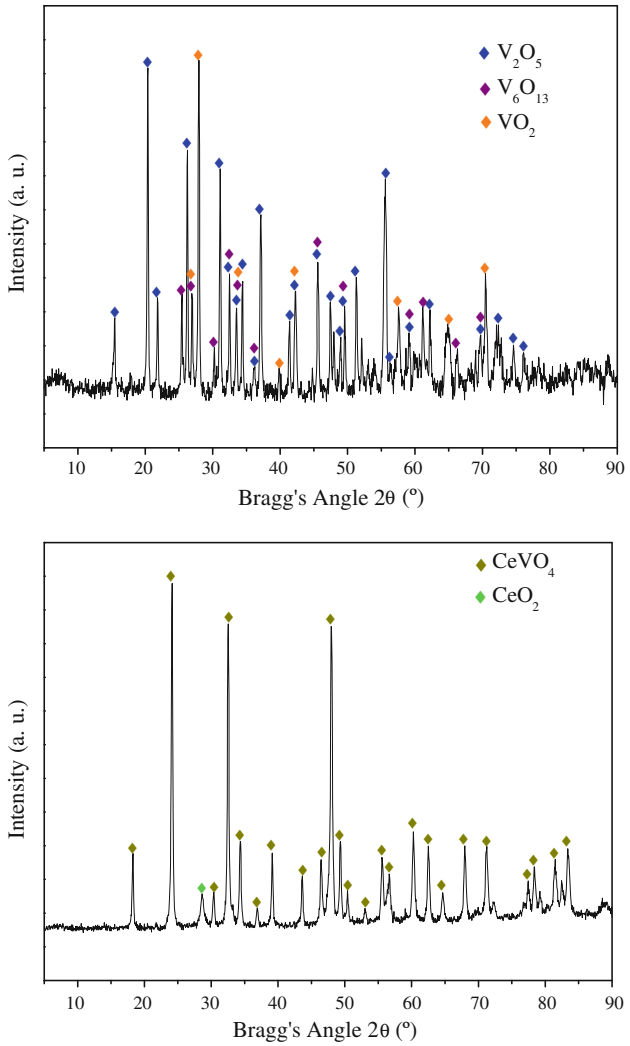

Fig. 9 XRD patterns of the V_2O_5 (*top*) and CeV (*bottom*) catalysts after reaction tests. Symbols: (♦) $CeVO_4$ (JCPDS12-757), (♦) CeO_2 (JCPDS34-394 (♦) V_2O_5 (JCPDS41-1426), (♦) VO_2 (JCPDS43-1051), (♦) V_6O_{13} (JCPDS27-1318)

Table 5 XRD parameters of the samples after catalytic tests

Sample	(hkl)[a]	d_{hkl} (nm)[b]	L (nm)[c]
V_2O_5	(001)	0.435	54.4 ± 2.0
CeV	(200)	0.368	39.8 ± 1.7

[a] Miller indices, [b] interplanar distance, [c] crystallite size

[21] that disappeared on the used sample. It confirms that these surface species were reduced to CeO_{2-x} species at the surface. In addition we did not observe any carbon formation at the surface after reaction.

Therefore, it suggests that there is an inhibition effect of the surface species. We may explain this inhibition effect by the reduction of surface CeO_2 species by CO formation during the reaction with time on stream which is in accordance with Trovarelli et al. [13]:

$$CeO_2 + xCO \rightarrow CeO_{2-x} + xCO_2 \quad (1)$$

$$CeO_2 + C_xH_y \rightarrow CeO_{2-(2x+0.5y)} + xCO_2 + 0.5yH_2O \quad (2)$$

$$CeO_2 + xH_2 \rightarrow CeO_{2-x} + xH_2O \quad (3)$$

$$CeO_{2-x} + xH_2O \rightarrow CeO_2 + xH_2 \quad (4)$$

$$CeO_{2-x} + 0.5xO_2 \rightarrow CeO_2 \quad (5)$$

Indeed, the oxygen supply is insufficient to restore the CeO_2 species and the vacancies are not restored due to the formation of several intermediate cerium species at the surface, decreasing very fast the reactivity after running several hours. Therefore, besides the promoting effect of oxygen from the vacancies, there is a strong inhibition effect with the formation of inactive species during the reaction process, evidencing strong modification of the surface species of the mixed oxide, although the higher initial activity and selectivity. Notwithstanding is the higher and stable selectivity toward H_2 as shown in Fig. 8, which is attributed to the presence of water, according to Eq. 4.

5 Conclusions

Catalytic tests have shown that (CeV) mixed oxide was more active than the vanadium oxide (V_2O_5) but both exhibited significant deactivation during the reaction. Both catalysts showed similar hydrogen selectivity with time on stream. On the other hand, the cerium oxide activity was very stable with time on stream, exhibiting very low hydrogen selectivity.

XRD patterns of the (CeV) mixed oxide showed the formation of 87 % of $CeVO_4$ phase and 13 % of CeO_2 phase, probably because of the hard solubilization of NH_4VO_3. Furthermore, the two preparations evidenced reproducibility of the synthesis of mixed oxide.

Incorporation of vanadium into the ceria structure improved the redox ability of ceria as shown by reversibility through TPR–TPO measurements, inhibiting the formation of carbon species on surface of the $CeVO_4$ as shown in the TG analysis.

The XRD diffractograms of V_2O_5 after reaction showed sintering of V_2O_5 and different oxidation states after reaction, affecting the surface active sites. On the contrary, the mixed oxide $CeVO_4$ crystallites remained unchanged. However the deactivation of the mixed oxide (CeV) with time on stream can be assigned to the insufficient oxygen supply to restore the CeO_2 species and the vacancies which are not restored due to the formation of several intermediate cerium species at the surface.

Acknowledgments The authors thank Marta Cristina Amorim and Carlos André Perez for the discussions on FEG and XRD analyses;

CNPq (Conselho Nacional de Desenvolvimento Científico) and FAPERJ (Fundação de Amparo à Pesquisa do Estado do Rio de Janeiro) for the scholarship (C.A.C) and Research Funding's.

References

1. Pena MA, Gomes JP (1996) J.L.G Fierro. Appl Catal A 144:7
2. Armor J (1999) Appl Catal A 176:159
3. Ahmed S, Kumar R, Krumpelt M (1999) Fuel Cells Bull 2:4
4. Wang X, Wang N, Wang L (2011) Int J Hydrogen Energy 36:466
5. Silberova B, Venvik J, Holmen A (2005) Catal Today 99:69
6. Corbo P, Migliardini F (2007) Int J Hydrogen Energy 32:55
7. Dady B, Das T, Kugler E (2011) Appl Catal A 392:127
8. Wang G, Meng M, Zha Y, Ding T (2010) Fuel 89:2244
9. Liu S, Xu L, Xie S, Wang Q, Xiong G (2001) Appl Catal A 211:145
10. Ayabe S, Omoto H, Utaka T, Kikuchi R, Sasaki K, Teraoka Y, Eguchi K (2003) Appl Catal A 241:261
11. Trimm L (1999) Catal Today 49:3
12. Fornasiero P, Balducci G, Monte R, Kaspar J (1996) V Sergo, G. Gubitosa, A. Ferrero, M. Graziani. J Catal 164:173
13. Trovarelli A, Leitenburg C, Boaro M, Dolcetti G (1999) Catal Today 50:353
14. Ballarini N, Battisti A, Cavani F, Cericola A, Cortelli C, Ferrari M, Trifiro F, Arpentinier P (2006) Appl Catal A 307:148
15. Laosiripojana N, Assabumrungrat S (2006) J Power Sources 158:348
16. Yasyerli S, Dogu G, Dogu T (2006) Catal Today 117:271
17. Rietveld HM (1969) J Appl Cryst 2:65
18. Leofanti G, Padovan M, Tozzola G, Venturelli B (1998) Catal Today 41:207
19. Ballarini N, Battisti A, Cavani F, Cericola A, Lucarelli C, Racioppi S, Arpentinier P (2006) Catal Today 116:313
20. Laosiripojana N, Sutthisripok W, Kim-Lohsoontorn P, Assabumrungrat S (2010) Int J Hydrogen Energy 35:6747
21. Jiminez C, Caroff T, Bartasyte A, Margueron S, Abrutis A, Chaix-Pluchery O, Weiss F (2009) Appl Spectrosc 63:401